HiLL PUBLISHING

Engineering Advances, 2023, 3(5), 387-394
https://www.hillpublisher.com/journals/ea/
ISSN Online: 2768-7961

Structural Characterization of Multi-doped Barium Cerate as Perovskite for Solid Oxide Fuel Cells

S. Hossain[1,*], M. S. Islam[1,*], S. A. Lopa[2], A. M. Abdalla[3], A. K. Azad[4]

[1]Institute of Nuclear Science and Technology, Bangladesh Atomic Energy Commission, Dhaka, Bangladesh.
[2]International Image Management Ltd., Pragati Sorani, Dhaka, Bangladesh.
[3]Department of Mechanical Engineering, Faculty of Engineering, Suez Canal University, Ismailia, Egypt.
[4]Faculty of Integrated Technologies, Universiti Brunei Darussalam, Jalan Tungku Link, Gadong BE1410, Brunei Darussalam.

How to cite this paper: S. Hossain, M. S. Islam, S. A. Lopa, A. M. Abdalla, A. K. Azad. (2023) Structural Characterization of Multi-doped Barium Cerate as Perovskite for Solid Oxide Fuel Cells. *Engineering Advances*, 3(5), 387-394.
DOI: 10.26855/ea.2023.10.001

Received: September 22, 2023
Accepted: October 18, 2023
Published: November 10, 2023

***Corresponding author:** S. Hossain, Institute of Nuclear Science and Technology, Bangladesh Atomic Energy Commission, Dhaka, Bangladesh; M. S. Islam, Institute of Nuclear Science and Technology, Bangladesh Atomic Energy Commission, Dhaka, Bangladesh.

Abstract

Perovskite type material $BaCe_{0.65}Zr_{0.10}Y_{0.05}Pr_{0.20}O_{3-\delta}$ was synthesized by the conventional solid-state reaction method with a sintering temperature of 1350°C for 8 hours in an air atmosphere. The structural, morphological, and thermal characterizations have been performed using X-ray diffraction (XRD), Scanning Electron Microscopy (SEM), Thermogravimetric Analysis (TGA), and Differential Thermal Analysis (DTA). From Rietveld refinement, we confirmed that our prepared sample was an orthorhombic crystal structure in the Pbnm space group. From TG/DTA, we get a gradual weight gain from 150ºC to 780ºC and a sharp weight loss after the temperature of 780ºC. The SEM image of the pellet surface of the sample shows that the sample sintered at 1350ºC was dense and suitable to use as an electrolyte in solid oxide fuel cells (SOFCs).

Keywords

Perovskite, protonic conductor, oxygen vacancy, space group, Rietveld refinement

1. Introduction

Intermediate temperature solid-oxide fuel cells (IT-SOFCs) have the possibility of long-term stability and economic competitiveness for various applications. For that reason, a lot of interest has been given to intermediate temperature solid-oxide fuel cells (IT-SOFCs) worldwide [1-7]. Doped ceria now looks to be the best electrolyte material available, perhaps meeting the majority of criteria for fuel-cell functioning below 600°C [8]. Some significant issues remain, however, including electronic conductivity and undefined mechanical integrity under fuel-cell functional conditions. Now, the main challenge in the SOFC community is the investigation of a new solid electrolyte for low-temperature SOFCs. For low-temperature SOFCs, proton conductors provide promising possibilities for electrolytes. This is because of their low activation energy of proton conduction. In a reducing environment, several perovskite-type oxides have strong proton conductivity [9-12]. Finding an appropriate approach between conductivity and chemical stability is one of the most important challenges for this type of proton conductor [13-15]. Such as, doped $BaCeO_3$ has inadequate chemical stability in a CO_2 and H_2O containing atmosphere for fuel-cell applications but it has enough high ionic conductivity.

As solid solutions are easily formed from $BaCeO_3$ and $BaZrO_3$, we can displace a desired fraction of Ce in $BaCeO_3$ with Zr to form a solid solution. As a result, the new form of $BaCeO_3$ exhibits both adequate proton conductivity as well as sufficient thermal and chemical stability over a large range of circumstances relevant to fuel cell operation [9, 16-18]. Doped zirconates have higher chemical stability than doped cerates but poorer conductivity. The introduction of Zr at B site enhances the stability of doped barium cerate. On the other hand, chemical and thermal stability also improve in a broad range of conditions referring to the fuel-cell operation. It is difficult to produce of an electrolyte with a high density and high sintering temperatures. In order to improve sinterability, Babilo and Haile [19] and Tao and Irvine [20]

introduced Zn into Y and Zr doped $BaCeO_3$. Another reports [21, 22] showed the stable proton-conducting electrolyte $BaCe_{0.5}Zr_{0.3}Y_{0.16}Zn_{0.04}O_{3-\delta}$ and $BaCe_{0.7}Zr_{0.1}Y_{0.05}Zn_{0.15}O_3$ by co-doping of Zr and Zn in the lattice could be sintered densely at lower temperatures [22] and the chemical stability was also improved. In this work we substitute cerium by zirconium, yttrium and praseodymium. In comparison to prior efforts in the literature, the composition was produced as a single-phase perovskite and its structural and thermal characteristics were examined. The conductivity of proton through the electrolyte is mainly dependent on the concentration of oxygen vacancies in the perovskites oxides. The vacancies of oxygen in these oxides can be significantly improved by acceptor doping, i.e., doping at the B-site by lower valance elements (LVE), typically yttrium or other rare earth metals [23].

During the synthesis process and the operation of the SOFC cell, the following two reactions may take place in the presence of oxygen:

$$2Ce_{Ce}^{X} + O_o^{X} + M_2O_3 \rightarrow 2M_{Ce}^{'} + V_o^{"} + 2CeO_2 \quad (1)$$

$$\frac{1}{2}O_2 + V_o^{"} \rightarrow O_o^{X} + 2h \quad (2)$$

The following mechanism has been proposed for the incorporation of protons in a hydrogen or water rich atmosphere and their conduction [24-26],

$$H_2O_{(g)} + V_o^{"} + O_o^{X} \rightarrow 2OH_o^{'} \quad (3)$$

The significance of this research work is to developing intermediate-temperature (500-700ºC) ceramic protons conductor as an anode support and electrolyte with a lower temperature and for adequate proton conductivity to meet the commercial target of reversible SOFCs and finding compatible electrodes with optimized functionality for dual-mode operation of reversible SOFCs.

Solid state reaction approach was used in this work to create the sample since it is frequently used to make ceramic compounds due to its low production cost and simplicity. Many investigators have employed solid-state reactions to synthesize oxides pertinent to IT-SOFCs [20, 27-29] and spinel ferrite [30-34].

2. Experimental design

$BaCe_{0.65}Zr_{0.10}Y_{0.05}Pr_{0.20}O_{3-\delta}$(BCZYP) was prepared by the conventional solid state reaction method. The total amount of sample was 10gm. The sample was sintered at 1350°C for 8 hours inside a muffle furnace (box furnace, Model: ST-1700 MX-III). The ingredients chemicals (purity more than 99.95%) $BaCO_3$, CeO_2, ZrO_2, Y_2O_3 and Pr_6O_{11}supplied from the company Sigma Aldrich were used as initial chemicals in precise stoichiometric ratios. A precise digital microbalance (Model: AND, GR-200) was used to precisely weigh each powder before they were fully combined for an hour in an agate mortar (made of fine stone). The sample was then milled intimately using a ball-mill machine (Paul O. Abbe Inc., Model 202421) for about 6 hours with appropriate amount of ethanol and then was dried on a magnetic heater (Stuart, Model: SB 162) with stirring. Disc-shaped pellets of 2 g were made into a 13 mm dia stainless steel die under a Hydraulic press (Hydraulic Bench Press, Kennedy, Model: HBP 010) with a pressure of 30 MPa. The pellets were then fired at 900°C for 12 hours inside the muffle furnace with a heating and cooling rate of 5°C/min. Then the calcinated sample was ground in a mortar pestle for one hour and then mixed with a small amount of poly vinyl alcohol (PVA) as a binder and then ground again for about 30 minutes and finally pressed into the pellets of 2 g of 13 mm dia under the hydraulic press of 30 MPa pressure and heated again at a temperature 1200°C for 10 hours. After that it was again ground and pressed into pellets and then the pellets of the sample were finally sintered at 1350°C for 8 hours inside the furnace. For structural analysis the X-ray diffraction experiment was done on the sample using D8 Advanced Bruker XRD system with CuKα radiation of wavelength $\lambda = 1.5406$ Å in the angular range of $2\theta = 20^o$ to 80^o with a step size of 0.02^o at room temperature. The programs TREOR90 [35] and *Checkcell* [36] were used for indexing and refinement of the lattice parameters. The XRD data were analyzed using *FullProf* [37] suite program. The Scanning Electron Microscopy (SEM) experiments were carried out with a high-resolution SEM machine (Model: JSM-7610F, OXFORD); with SEI DETECTOR and ACCEL Voltage 5.00 Volt and the images were taken in different magnifications for getting better fracture images. A SETARAM TG-DTA/DSC thermogravimetric analyzer was used for the thermogravimetric analysis (TGA) of the sample. In the TG furnace, the sample was heated to 900°C in dry argon at a rate of 10°C/min. TGA in pure Ar was carried out on at 10°C/min from 20 to 900°C, held isothermally for 90 min, and then cooled down to 20°C at the same rate, with flowing the same gas.

3. Results and Discussion

3.1 XRD Pattern Analysis

Figure 1 below displays the Rietveld analysis of $BaCe_{0.65}Zr_{0.10}Y_{0.05}Pr_{0.20}O_{3-\delta}$XRD spectra at room temperature after sintering at 1350°C.

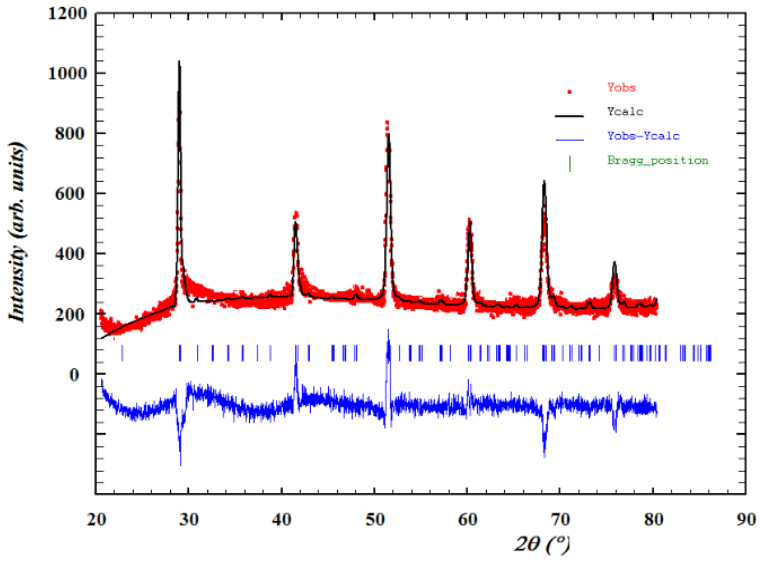

Figure 1. Rietveld analysis profile of X- ray diffraction pattern of as- prepared $BaCe_{0.65}Zr_{0.10}Y_{0.05}Pr_{0.20}O_{3-\delta}$ at room temperature.

The single-phase perovskite structure was confirmed by the Rietveld analysis of the X-ray diffraction pattern. The observed data, calculated data, difference between the observed and calculated data, and Bragg locations are each displayed in the XRD pattern.

In Figure 2, it is shown the Bragg positions and their respective (hkl) values of $BaCe_{0.65}Zr_{0.10}Y_{0.05}Pr_{0.20}O_{3-\delta}$ at room temperature after the Rietveld analysis of the XRD data.

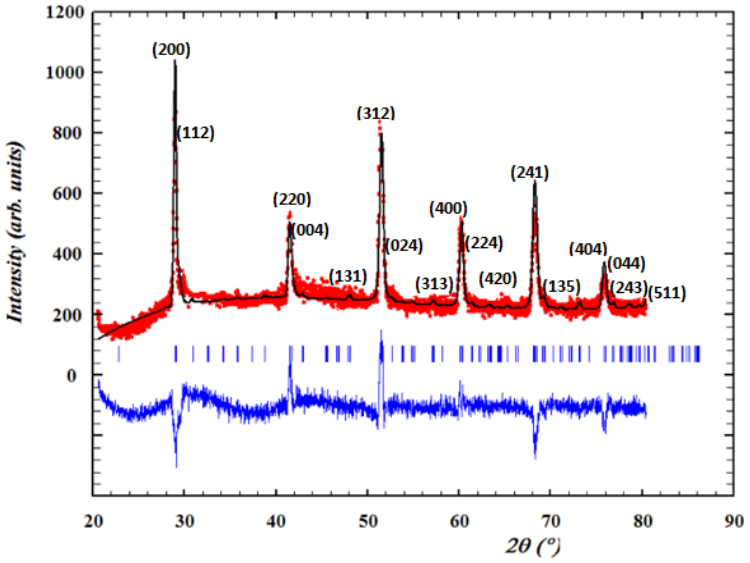

Figure 2. The significant Bragg positions and their respective (hkl) values of BCZYP after the Rietveld analysis of XRD data.

The significant Bragg positions and their respective (hkl) values are 28.9922 (2 0 0), 29.1072 (1 1 2), 41.5520 (2 2 0), 41.7155 (0 0 4), 48.0396 (1 3 1), 51.4582 (3 1 2), 51.6735 (0 2 4), 57.0536 (3 1 3), 60.0827 (4 0 0), 60.3412 (2 2 4), 68.1333 (4 2 0), 69.2925 (2 4 1), 73.2423 (1 3 5), 75.8051(4 0 4), 76.0413 (0 4 4), 76.8894 (2 4 3) and 80.2484 (5 1 1) which are shown in the Reitvelt refinement XRD pattern of Figure 2.

Figure 3 (a) shows the polyhedral shape and Figure 3 (b) shows the schematic 3D ball and stick diagram of the materialafter the refinement. In Figure 3 (a), it shows that the barium atom is at the center and oxygen are at the edges of each shape same as the perovskite (ABO_3) oxide shape.

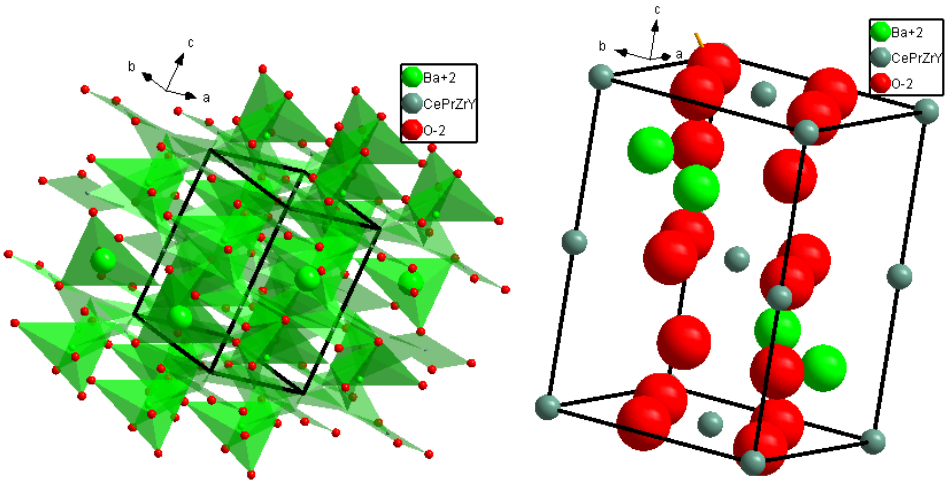

(a) (b)

Figure 3. (a) Polyhedral shape and (b) Schematic 3D ball and stick diagram of the material after the refinement.

The orthorhombic structure with the space group Pbnm can be observed in the XRD study of BCZYP, and this space group was finally chosen in the data refining procedure to generate the estimated diffraction profiles after being validated with a few alternative crystal structures and space groups. Table 1 contains a list of the refinement parameters.

Table 1. Crystallographic information's from Rietveld analysis of the XRD data of BCZYP

Quantity	Results
Unit cell parameters (Å)	a = 6.1506(4), b = 6.1362(8), c = 8.6532(4) and α = β = γ = 90°
Space group	Pbnm
Atomic fractional coordinates	Ba (0.5076,0.0235,0.250); Ce/Zr/Y/Pr (0,0,0); O1 (0.352,0.574,0.250) and O_2 (0.286,0.353,0.256)
Oxygen occupancy	97%
R-factors (%)	R_p: 8.64, R_{wp}: 9.93, R_{exp}: 8.41, Chi^2: 3.15

The contour 2D picture of the sample in which one atom (barium) is in the middle of the structure and other are bonded with barium in a very regular arrangement is shows in Figure 4. We are able to conclude that the sample's synthesis was precise based on its arrangement.

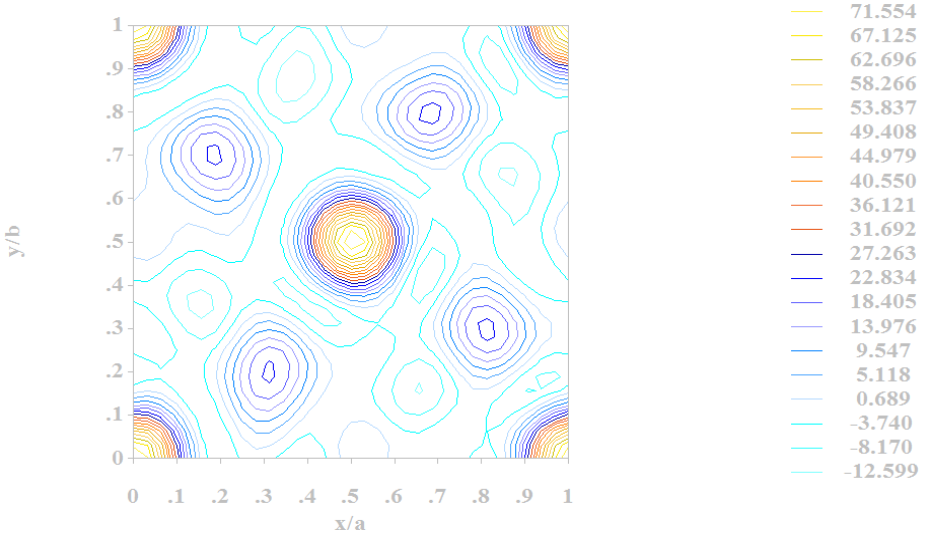

Figure 4. Contour 2D diagram of BCZYP after the Rietveld analysis of XRD data.

The contour 3D diagram is shown in Figure 5 (a) where the electron density of the BCZYP is shown. In the synthesized material, it is seen that the central atom which contains more than 71% electrons which tells that the biggest atom took the place at the center position as the perovskite oxide structure. In Figure 5 (b), it shows the iso-surface of BCZYP that represents points of the constant value (e.g. pressure, temperature, velocity, density) of the material within the volume of space; in other words, it is a level set of a continuous function whose domain is 3D-space in this composition of perovskite structure. These figures showed that after the synthesis all constitutes atoms takes the right positions as a peovskite structure.

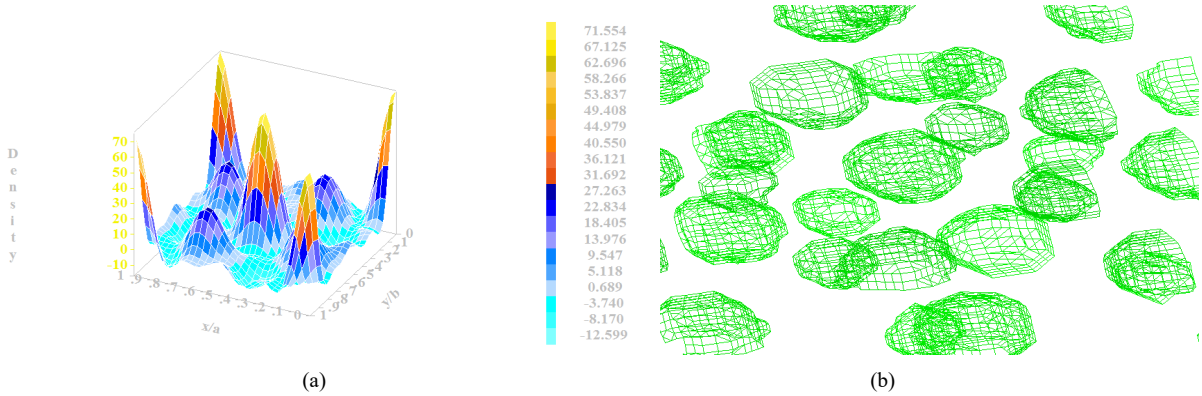

(a) (b)

Figure 5. (a) Contour 3D diagram and (b) Iso-surface diagram of BCZYP at RT.

3.2 Scanning Electron Microscopy (SEM)

The SEM of $BaCe_{0.65}Zr_{0.10}Y_{0.05}Pr_{0.20}O_{3-\delta}$ (BCZYP) shows up in Figure 6 at the magnifications shown at the bottom of the BCZYP image. According to the SEM picture of the fracture surface of our reported sample sintered at 1350°C, it was a dense sample with no identifiable pores or crakes.

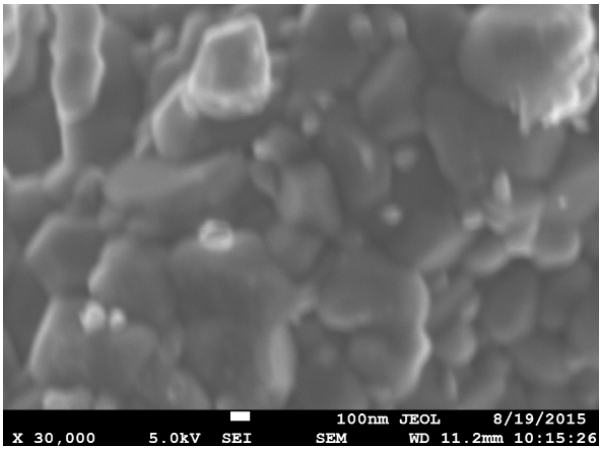

Figure 6. SEM of $BaCe_{0.65}Zr_{0.10}Y_{0.05}Pr_{0.20}O_{3-\delta}$ as-prepared sample sintered at 1350°C.

The bimodal microstructure of the pure BCZYP contained two sizes of grains, the bigger grains and other smaller grains, as can be seen in SEM image 6.

The sizes of the bigger grains are 0.4-0.5 μm and smaller 0.2-0.3 μm respectively. The grain size on praseodymium substitution has been shown to be uniform. In comparison to Zr rich compositions; ceria rich compositions had bigger average grains. It indicates that the general grain size distribution is influenced by the type of dopant. The larger grain size of the sample offers less overall grain boundary resistance and the smaller grain size of the sample gives high overall grain boundary resistance.

3.3 Thermogravimetric Analysis (TGA)

The temperature vs mass change graph is shown in Figure 7. Throughout the experiment's increasing and lowering temperatures, the heat flow versus temperature remained almost constant. From this figure we observe that mass is decreasing at 100°C to 150°C and then gradually increases up to 900°C during the heating process of the sample under the argon gas environment. This is comparable to the protonic conducting behavior of the materials used in IT-SOFCs.

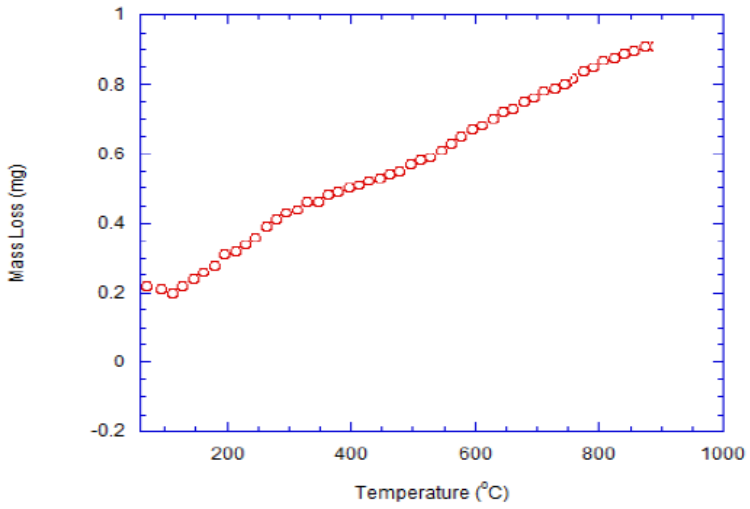

Figure 7. TGA of $BaCe_{0.65}Zr_{0.01}Y_{0.05}Pr_{0.20}O_{3-\delta}$ prepared by the solid state sintering method under Ar flow.

The TGA measurement shows a two stages weight loss. In the case of argon, the initial weight loss takes place in between 100ºC and 150°C and there is weight loss until 910ºC. Weight increased because of protonic conducting behavior between 150°C and 900°C. In this temperature range, the mass could increase due to the proton uptake from the stream (H_2O), containing in atmosphere (air) because the sample chamber of this TGA system is not completely isolated from the environment. At high temperatures or in a reducing environment, lattice oxygen may lose, forming oxygen vacancies for possible oxygen migration.

4. Conclusions

A single-phase orthorhombic structure with Pbnm space group is confirmed to our perovskite sample prepared in the solid-state ceramic method at a lower temperature than others in literature from the X-ray diffraction pattern. From the SEM picture, it is clear that our sample doesn't have pore and crack with highly dense in nature. The solid-state reaction method with the sintering temperature 1350°C can produce our desire sample is observed from the TG-DTA analysis. From the studied properties of the materials, it can say that the materials can be the potential candidate as the electrolyte as the proton conductor.

References

[1] E. Fabbri, D. Pergolesi, and E. Traversa. "Materials challenges toward proton-conducting oxide fuel cells: a critical review." *Chem. Soc. Rev.*, vol. 39, no. 11, p. 4355, 2010, doi: 10.1039/b902343g.

[2] C. Duan, et al. "Readily processed protonic ceramic fuel cells with high performance at low temperatures." *Sci.*, vol. 349, no. 6254, pp. 1321–1326, Sep. 2015, doi: 10.1126/science.aab3987.

[3] E. C. C. de Souza and R. Muccillo. "Properties and applications of perovskite proton conductors." *Mater. Res.*, vol. 13, no. 3, pp. 385–394, Sep. 2010, doi: 10.1590/S1516-14392010000300018.

[4] R. Haugsrud and T. Norby. "Proton conduction in rare-earth ortho-niobates and ortho-tantalates." *Nat. Mater.*, vol. 5, no. 3, pp. 193–196, Mar. 2006, doi: 10.1038/nmat1591.

[5] R. N. Karnik. "Materials science: Breakthrough for protons." *Nature*, vol. 516, no. 7530, pp. 173–175, Dec. 2014.

[6] P. Qiu, et al. "LaCrO 3 -Coated La 0.6 Sr 0.4 Co 0.2 Fe 0.8 O 3−δ Core–Shell Structured Cathode with Enhanced Cr Tolerance for Intermediate-Temperature Solid Oxide Fuel Cells." *ACS Appl. Mater. Interfaces*, p. acsami.0c01962, Jun. 2020, doi: 10.1021/acsami.0c01962.

[7] S.-L. Zhang, et al. "Cobalt-substituted SrTi 0.3 Fe 0.7 O 3−δ : a stable high-performance oxygen electrode material for intermediate-temperature solid oxide electrochemical cells." *Energy Environ. Sci.*, vol. 11, no. 7, pp. 1870–1879, 2018, doi: 10.1039/C8EE00449H.

[8] Z. Shi, W. Sun, and W. Liu, "Synthesis and characterization of BaZr0.3Ce0.5Y0.2−xYbxO3−δ proton conductor for solid oxide fuel cells." *J. Power Sources*, vol. 245, pp. 953–957, Jan. 2014, doi: 10.1016/j.jpowsour.2013.07.060.

[9] K. Katahira, Y. Kohchi, T. Shimura, and H. Iwahara. "Protonic conduction in Zr-substituted BaCeO3." *Solid State Ionics*, vol. 138, no. 1–2, pp. 91–98, Dec. 2000, doi: 10.1016/S0167-2738(00)00777-3.

[10] A. K. Azad and J. T. S. Irvine. "High density and low temperature sintered proton conductor BaCe0.5Zr0.35Sc0.1Zn0.05O3-delta." *Solid State Ionics*, vol. 179, no. 19–20, pp. 678–682, 2008, doi: DOI 10.1016/j.ssi.2008.04.036.

[11] R. Kannan, K. Singh, S. Gill, T. Fürstenhaupt, and V. Thangadurai. "Chemically stable proton conducting doped $BaCeO_3$ -no more fear to SOFC wastes." *Sci. Rep.*, vol. 3, p. 2138, 2013, doi: 10.1038/srep02138.

[12] H. Kawamori, I. Oikawa, and H. Takamura. "Protonation-Induced B -Site Deficiency in Perovskite-Type Oxides: Fully Hydrated BaSc 0.67 O(OH) 2 as a Proton Conductor." *Chem. Mater.*, vol. 33, no. 15, pp. 5935–5942, Aug. 2021, doi: 10.1021/acs.chemmater.1c01017.

[13] J. Lv, L. Wang, D. Lei, H. Guo, and R. V Kumar. "Sintering, chemical stability and electrical conductivity of the perovskite proton conductors BaCe0.45Zr0.45M0.1O3−δ (M = In, Y, Gd, Sm)." *J. Alloys Compd.*, vol. 467, no. 1–2, pp. 376–382, 2009, doi: http://dx.doi.org/10.1016/j.jallcom.2007.12.103.

[14] A. K. Azad and J. T. S. Irvine. "Synthesis, chemical stability and proton conductivity of the perovksites Ba(Ce,Zr)(1-x)Sc-x O3-delta." *Solid State Ionics*, vol. 178, no. 7–10, pp. 635–640, 2007, doi: DOI 10.1016/j.ssi.2007.02.004.

[15] P. Sawant, S. Varma, B. N. Wani, and S. R. Bharadwaj. "Synthesis, stability and conductivity of BaCe0.8−xZrxY0.2O3−δ as electrolyte for proton conducting SOFC." *Int. J. Hydrogen Energy*, vol. 37, no. 4, pp. 3848–3856, 2012, doi: 10.1016/j.ijhydene.2011.04.106.

[16] D. A. Stevenson, N. Jiang, R. M. Buchanan, and F. E. G. Henn. "Characterization of Gd, Yb and Nd doped barium cerates as proton conductors." *Solid State Ionics*, vol. 62, no. 3–4, pp. 279–285, 1993, doi: http://dx.doi.org/10.1016/0167-2738(93)90383-E.

[17] A. K. Azad, A. Kruth, and J. T. S. Irvine. "Influence of atmosphere on redox structure of BaCe0.9Y0.1O2.95 – Insight from neutron diffraction study," *Int. J. Hydrogen Energy*, vol. 39, no. 24, pp. 12804–12811, Aug. 2014, doi: 10.1016/j.ijhydene.2014.05.080.

[18] A. K. Azad, D. D. Y. Setsoafia, L. C. Ming, and P. M. I. Petra. "Synthesis and characterization of high density and low temperature sintered proton conductor BaCe0.5Zr0.35In0.1Zn0.05O3-d." *Adv. Mater. Res.*, vol. 1098, pp. 104–109, 2015.

[19] P. Babilo and S. M. Haile. "Enhanced sintering of yttrium-doped barium zirconate by addition of ZnO." *J. Am. Ceram. Soc.*, vol. 88, no. 9, pp. 2362–2368, 2005, doi: 10.1111/j.1551-2916.2005.00449.x.

[20] S. Tao and J. T. S. Irvine. "A stable, easily sintered proton-conducting oxide electrolyte for moderate-temperature fuel cells and electrolyzers." *Adv. Mater.*, vol. 18, no. 12, pp. 1581–1584, 2006.

[21] X. Lu, Y. Ding, and Y. Chen. "Ba0.5Sr0.5Zn0.2Fe0.8O3−δ–BaCe0.5Zr0.3Y0.16Zn0.04O3−δ composite cathode for proton-conducting solid oxide fuel cells." *J. Alloys Compd.*, vol. 484, no. 1–2, pp. 856–859, 2009, doi: 10.1016/j.jallcom.2009.05.065.

[22] S. Hossain, N. Radenahmad, J. H. Zaini, F. Begum, and A. K. Azad. "Structural, thermal and microstructural studies of the proton conductor BaCe 0.7 Zr 0.1 Y 0.05 Zn 0.15 O 3 for IT-SOFCs." *IOP Conf. Ser. Mater. Sci. Eng.*, vol. 121, p. 012014, Mar. 2016, doi: 10.1088/1757-899X/121/1/012014.

[23] N. Bonanos. "Oxide-based protonic conductors: point defects and transport properties." *Solid State Ionics*, vol. 145, no. 1–4, pp. 265–274, 2001, doi: http://dx.doi.org/10.1016/S0167-2738(01)00951-1.

[24] R. Glöckner, M. S. Islam, and T. Norby. "Protons and other defects in BaCeO3: a computational study," *Solid State Ionics*, vol. 122, no. 1–4, pp. 145–156, 1999, doi: http://dx.doi.org/10.1016/S0167-2738(99)00070-3.

[25] I. Ahmed, et al. "Location of deuteron sites in the proton conducting perovskite BaZr0.50In0.50O3−y." *J. Alloys Compd.*, vol. 450, no. 1–2, pp. 103–110, 2008, doi: http://dx.doi.org/10.1016/j.jallcom.2006.11.154.

[26] A. K. Azad and J. T. S. Irvine. "Location of Deuterium Positions in the Proton-Conducting Perovskite BaCe 0.4 Zr 0.4 Sc 0.2 O 2.90 · x D 2 O by Neutron Powder Diffraction." *Chem. Mater.*, vol. 21, no. 2, pp. 215–222, Jan. 2009, doi: 10.1021/cm8031847.

[27] M. Miyake, M. Iwami, M. Takeuchi, S. Nishimoto, and Y. Kameshima. "Electrochemical performance of Ni0.8Cu0.2 /Ce0.8Gd0.2O1.9 cermet anodes with functionally graded structures for intermediate-temperature solid oxide fuel cell fueled with syngas." *J. Power Sources*, vol. 390, pp. 181–185, Jun. 2018, doi: 10.1016/j.jpowsour.2018.04.051.

[28] I. Ahmed, et al. "Crystal Structure and Proton Conductivity of BaZr0. 9Sc0. 1O3- δ." *J. Am. Ceram. Soc.*, vol. 91, no. 9, pp. 3039–3044, 2008.

[29] A. I. Klyndyuk, et al. "Double substituted NdBa(Fe,Co,Cu)2O5+δ layered perovskites as cathode materials for intermediate-temperature solid oxide fuel cells – correlation between structure and electrochemical properties." *Electrochim. Acta*, vol. 411, p. 140062, Apr. 2022, doi: 10.1016/j.electacta.2022.140062.

[30] S. Hossain, et al. "Preparation and Structural Properties of ZnAl x Fe 2 − x O 4 Spinel Oxide." no. February, pp. 203–209, 2016.

[31] L. Zhang, Y. Wang, B. Liu, J. Wang, G. Han, and Y. Zhang. "Characterization and property of magnetic ferrite ceramics with interesting multilayer structure prepared by solid-state reaction." *Ceram. Int.*, vol. 47, no. 8, pp. 10927–10939, Apr. 2021, doi: 10.1016/j.ceramint.2020.12.212.

[32] S. Hossain, M. K. Hasan, S. K. M. Yunus, A. K. M. Zakaria, T. K. Datta, and A. K. Azad. "Synthesis and Investigation of the

Structural Properties of Al^{3+} Doped Mg Ferrites." *Appl. Mech. Mater.*, vol. 789–790, pp. 48–52, Sep. 2015, doi: 10.4028/www.scientific.net/AMM.789-790.48.

[33] S. Khanam, et al. "Study of the Crystallographic and Magnetic Structure in the Nickel Substituted Cobalt Ferrites by Neutron Diffraction." *Mater. Sci. Appl.*, vol. 6, pp. 332–342, 2015, doi: 10.4236/msa.2015.64038.

[34] A. K. M. Zakaria, et al. "Cation distribution and crystallographic characterization of the spinel oxides MgCr x Fe 2Àx O 4 by neutron diffraction." *J. Alloys Compd.*, vol. 633, pp. 115–119, 2015, doi: 10.1016/j.jallcom.2015.01.179.

[35] P. E. Werner, L. Eriksson, and M. Westdahl. "TREOR, a semi-exhaustive trial-and-error powder indexing program for all symmetries." *J. Appl. Crystallogr.*, vol. 18, no. 5, pp. 367–370, 1985, doi: 10.1107/S0021889885010512.

[36] J. Lougier and B. Bochu. (n.d.). "'Checkcell: Graphical Powder Diffraction Indexing Cell and Space Group Assignment Software.'"

[37] J. Rodriguez-Carvajal. "Recent advances in magnetic structure determination by neutron powder diffraction + FullProf." *Phys. B Condens. Matter*, vol. 192, no. 1–2, p. 55, 1993.